GEANT MC Simulations for a Sampling Calorimeter

Andy Raj and Wolfgang Lorenzon

February 13, 2000

Abstract

GEANT Monte Carlo simulations have been performed for a sampling calorimeter consisting of scintillator and tungsten plates to use with the longitudinal polarimeter at HERA. In particular linearity, resolution and uniformity have been estimated for the prototype sampling calorimeter which was built in 1998. Based on these results combined with data collected at the DESY test beam, a new calorimeter was designed and additional properties were studied, i.e. the analyzing power A_0 was simulated using a Compton generator and realistic beam smearing parameters. The results have shown that such a sampling calorimeter is quite insensitive to horizontal beam motion of up to ± 15 mm, and therefore ideally suited as a Compton calorimeter for the longitudinal polarimeter at HERMES.

Contents

1 Introduction

We started out with simulating the linearity, resolution and uniformity of the prototype sampling calorimeter which was built in 1998 by Joachim Seibert from Freiburg University. The term 'uniformity' describes the response of the calorimeter to the position of the incident beam on the front face of the detector. Note, that sometimes the term 'acceptance' is erroneously used for it. The initial goal was to compare those results with data that were collected at the DESY test beam, and then, based on these results, design a new sampling calorimeter. Unfortunately, the asymmetric readout scheme of the prototype sampling calorimeter made it impossible to compare uniformity studies directly to the simulations that were performed with a perfectly symmetric detector. Some simple geometric models were considered to understand the energy uniformity of the asymmetric design, however, none of them proved reliable enough. Attempts to simulate the energy uniformity of the prototype sampling calorimeter were therefore dropped since we also did not know of any way to simulate scintillation light propagation in GEANT. The linearity of the prototype, on the other hand, was not affected by the asymmetric readout, and we were able to confirm the highly linear response of the prototype calorimeter. Also, the simulations were very useful to determine how a symmetric detector response would look like, and how that response would change if the dimension of the detector were changed.

Note, that no background from gas bremsstrahlung was included in the simulation. This is a valid approach for realistic calorimeter response studies, if the calorimeter is operated in the multi-Compton mode. It is based on our experience with operating the longitudinal polarimeter in the HERA tunnel. However, if one plans to operate the calorimeter in single-Compton mode, then the bremsstrahlung background has to be included. For comparison, it is much larger (800 kHz or 0.08 per bunch crossing) than the bremsstrahlung background encountered with the transverse polarimeter ($10 - 20$ kHz).

2 Prototype Sampling Calorimeter

2.1 Linearity

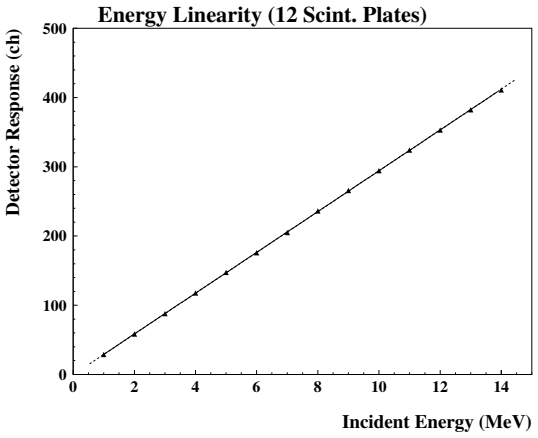

Figure 1. Linearity of the calorimeter for the 12 scintillator-tungsten configuration.

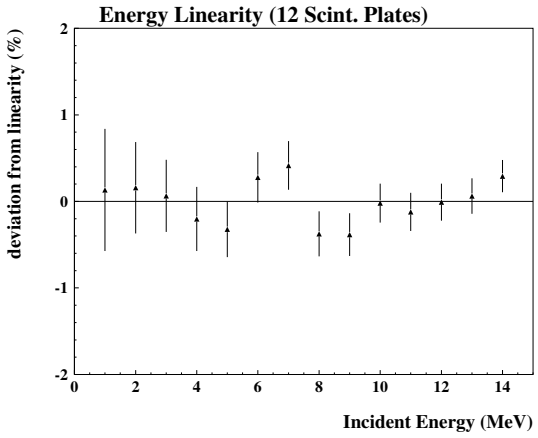

Figure 2. Deviation from linearity for the 12 scintillator-tungsten configuration.

The dimensions of the prototype sampling calorimeter, consisting of 12 tungsten and 12 scintillator plates, were 50.8 mm wide, 50.8 mm high, and 107.4 mm long. The linearity of the calorimeter

was tested with 12 scintillator plates, each 2.6-mm thick, sandwiched with 12 tungsten plates, each 6.35-mm thick. The incident gamma ray energy was varied from 1 Gev to 14 GeV in steps of 1 Gev. One thousand gamma rays were produced for each energy setting. The calorimeter was found to be highly linear. The linearity and the deviation from linearity obtained from the simulations are shown in Figs. 1 and 2. The gamma rays were incident as a point source at the center of the plates.

Simulations were also run for a configuration with 24 scintillator plates of thickness 2.6 mm and 24 tungsten plates of 3 mm thickness. The calorimeter was found to be linear over the entire range covered in this simulation. Fig. 3 and 4 show the linearity and the deviation from linearity for this configuration. Note, that the detector response is a factor 2.02 higher for the 24-plate configuration than for the 12-plate configuration. This is roughly what we expected since the total amount of scintillator material increased by about a factor of two, whereas the total thickness of the tungsten plates stayed almost constant.

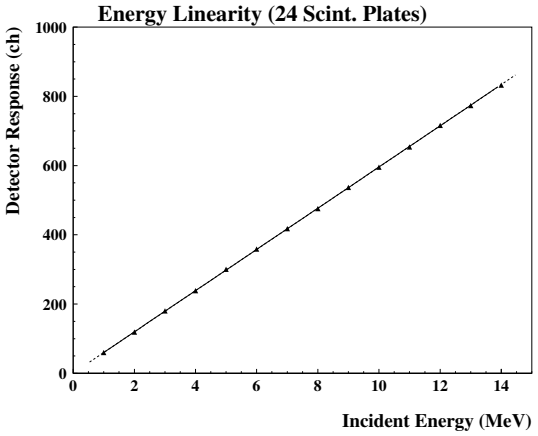

Figure 3. Linearity of the calorimeter for the 24 scintillator-tungsten configuration.

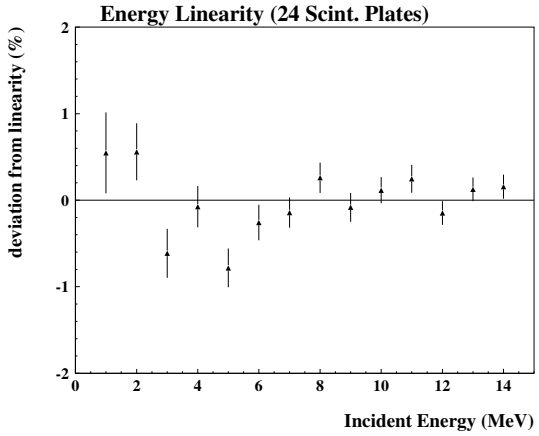

Figure 4. Deviation from linearity for the 24 scintillator-tungsten configuration.

2.2 Resolution

Figs. 5 and 6 show the resolution of the calorimeter for both the 12 and 24 scintillator and tungsten plate configurations. The line is a fit of the simulated data with a function

$$\frac{\sigma}{E} = \frac{a}{\sqrt{E}} + b, \tag{1}$$

which yields the values of $a \simeq 22.5\%$ and $b \simeq 0.204\%$ for the 12-plate configuration. The 24-plate configuration yielded the values of $a \simeq 14.4\%$ and $b \simeq 0.435\%$.

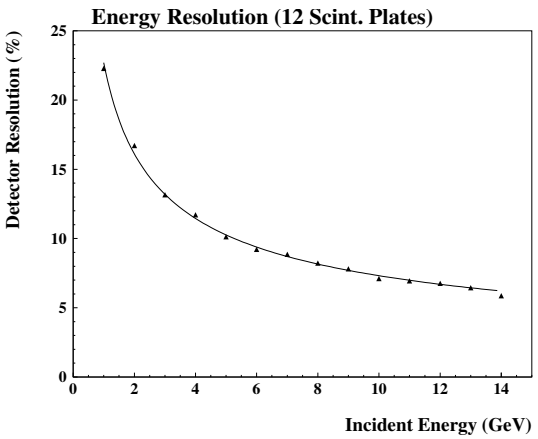

Figure 5. Resolution for the 12 scintillator-tungsten configuration.

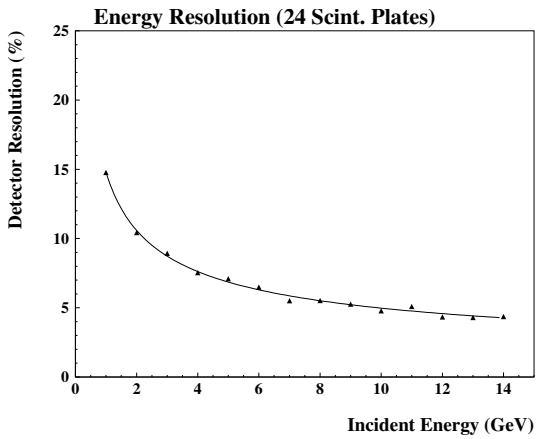

Figure 6. Resolution for the 24 scintillator-tungsten configuration.

2.3 Uniformity

Once the linearity and resolution were established, simulations were run by horizontally scanning the surface of the front plate of the 12 scintillator-tungsten configuration with 3 GeV gamma rays. This was done to test the sensitivity of the calorimeter to the position of the incident gamma rays. Fig. 7 shows that the response of the calorimeter was almost entirely flat over approximately ± 20 mm. However, it was found that at the edges the response was not symmetric, and the number of events recorded on one side was larger than the number on the other side. This was determined to be due to the back scattering from the tungsten plate placed on the right side of the scintillator-tungsten detector assembly (looking towards the direction of the gamma beam). These non-uniform edge effects can be avoided as desribed in Section 2.4.

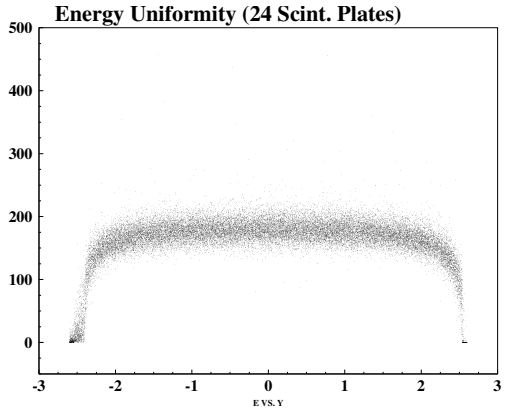

Figure 7. Uniformity of calorimeter using 3 GeV incident gamma rays. Plotted are the detector response (ch) as a function of incident gamma ray position (cm). On the right hand side, or at negative values of y, one can see the effect of having additional material surrounding the scintillator-tungsten plates.

2.4 Conclusions on Prototype

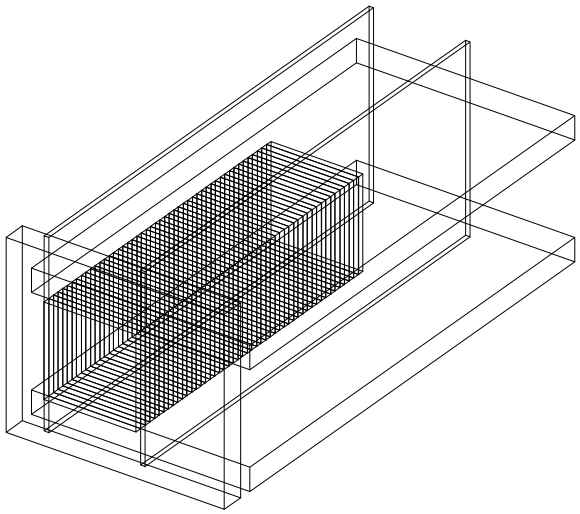

Figure 8. A 3-dim view of the scintillator-tungsten detector assembly, including the tungsten and aluminum side plates. Shown is the 24 scintillator-tungsten configuration.

From the above simulations it is concluded that the calorimeter is linear and the response is uniform within 5% in an approximately 30 mm x 30 mm area on the front face of the detector. Due to space constraints and requirements of a highly symmetric calorimeter, a new design of 40 mm x 40 mm was studied in more detail. Since the calorimeter response was not symmetric in the prototype (see Fig. 7), a tungsten plate was added to the left side (positive values of y) of the scintillator-tungsten detector. This can be seen in Fig. 8, which is a GEANT Monte Carlo view of the 24 scintillator-tungsten configuration that we decided to build. A 10-mm thick aluminum plate was also added to the top of the detector, again in an attempt to make the detector as symmetric as possible.

3 New Sampling Calorimeter

As mentioned in section 2.4, the new design was decided upon due to the space considerations and requirements of a highly symmetric calorimeter. We first repeated the same simulations that we had performed with the prototype to study the effects of reducing the lateral size of the detector. Due to better energy yield, the final design studies were only done for the 24 scintillator-tungsten configuration. These studies included a simulation of the analyzing power A_0 using a Compton generator and realistic beam smearing parameters.

3.1 Linearity and Resolution

The linearity of the calorimeter with the new dimensions was tested for the 12 and 24 scintillator-tungsten configurations. The widths and heights were kept constant at 40 mm x 40 mm. The thickness of the tungsten plates for the 12 (24) plate configuration were 6.35 mm (3 mm), and the thickness of the scintillator plates were 2.6 mm in both configurations. The incident gamma ray energy was varied again from 1 Gev to 14 GeV in steps of 1 Gev. The calorimeter response was found to be linear again within better than 1%. The deviation from linearity obtained from the

simulations are shown in Figs. 9 and 10. The gamma rays were also incident as a point source at the center of the plates.

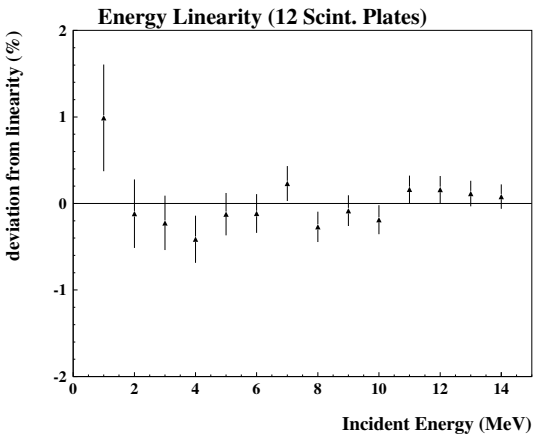

Figure 9. Deviation from linearity of the new design of the calorimeter with 12 scintillator plates sandwiched with 12 tungsten plates.

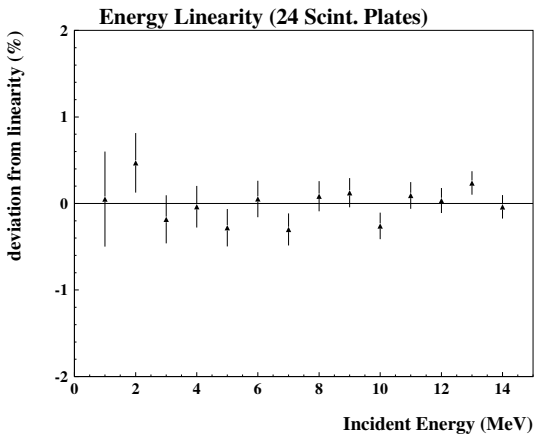

Figure 10. Deviation from linearity of the new design of the calorimeter with 24 scintillator plates sandwiched with 24 tungsten plates.

Figs. 11 and 12 show the resolution of the detector in the 12 and 24 scintillator-tungsten configurations, respectively. As expected the resolution of the calorimeter with 24 scintillator plates is better than that with 12 scintillator plates. The values of the fit parameters in Eq. 1 are $a \simeq 24.4\%$ and $b \simeq -0.160\%$ for the 12 plate configuration. The 24-plate configuration yielded the values of $a \simeq 15.6\%$ and $b \simeq 0.138\%$. If we compare these values with the values obtained for the 50.8 mm x 50.8 mm configuration (prototype sampling calorimeter), we find that the resolution got worse by approximately 8% for both, the 12 and the 24 plate configurations.

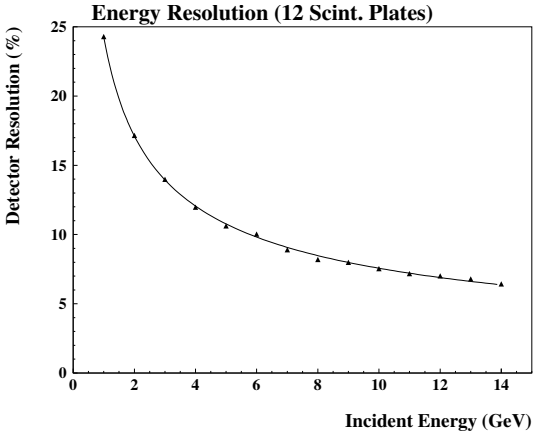

Figure 11. Resolution for the 12 scintillator-tungsten configuration of the new design.

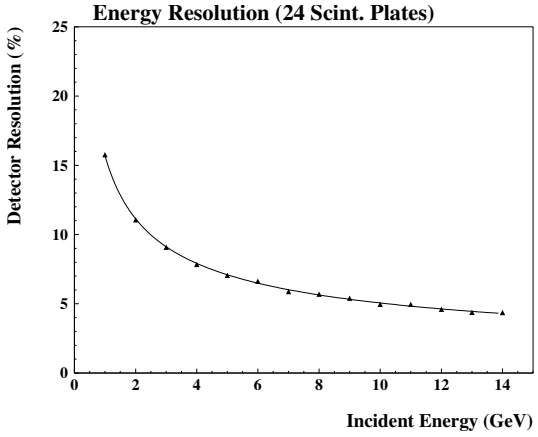

Figure 12. Resolution for the 24 scintillator-tungsten configuration of the new design.

3.2 Uniformity of Calorimeter

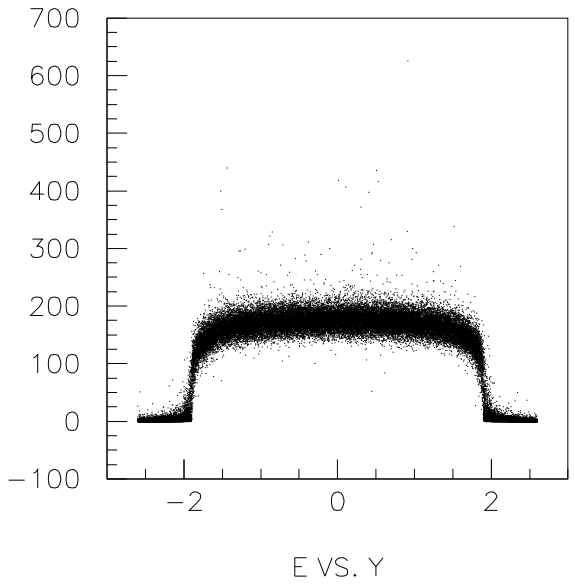

Figure 13. Uniformity of calorimeter using 3 GeV incident gamma rays for the 24 scintillator-tungsten configuration.

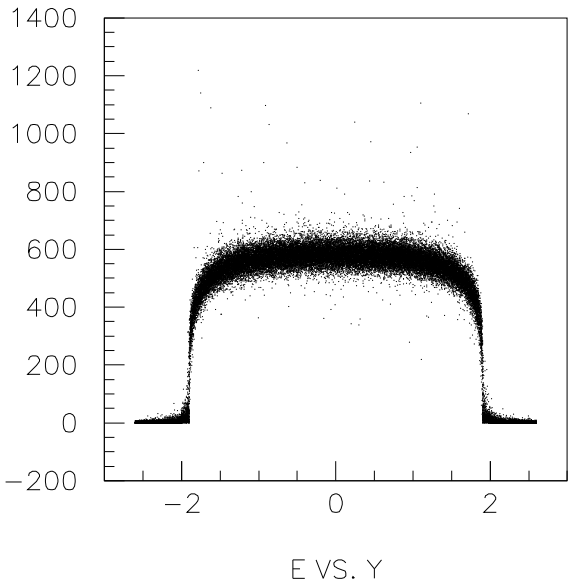

Figure 14. Uniformity of calorimeter using 10 GeV incident gamma rays for the 24 scintillator-tungsten configuration.

Since we opted for the 24 scintillator-tungsten configuration as the final design, we only present the uniformity studies for this particular configuration. We however wanted to check, whether there was a significant change in the uniformity for two different gamma ray energies. The comparison was done at 3 GeV and at 10 GeV. Fig. 13 displays the uniformity of the calorimeter for 3 GeV gamma rays. Fig. 14 shows the uniformity for 10 GeV gamma rays. These figures confirm that the response of the calorimeter is independent of energy, and flat within 5% (10%) for approximately $\pm$12 mm ($\pm$14 mm). Therefore, the Moliere radius in first order is independent of incident energy for this energy range, as expected. If the gamma rays move further away from the center, the detector response drops rapidly due to transverse leakage.

3.3 Conclusions on Linearity, Resolution and Uniformity

From the above simulations it was estimated that the calorimeter is linear and the response is uniform within 5% in an approximately 24 mm x 24 mm area on the front face of the detector for a configuration with 24 scintillator and tungsten plates, each 40 mm x 40 mm. The resolution of the 24 scintillator-tungsten configuration was much better than that of the 12 scintillator-tungsten configuration. The reduction of the lateral dimensions reduced the resolution only slightly (from 14.4% to 15.6%). Hence for the final design, the 24 scintillator-tungsten configuration was chosen.

3.4 Determination of Analyzing Power A_0

In order to study the sensitivity of the beam polarization measurement to beam motion, we rewrote the GEANT Monte Carlo code to include a Compton photon generator and realistic beam smearing parameters. In the previous simulations, we used a pencil beam that impinged on one position on the front face of the calorimeter, either in the center or at a well-defined location away from the center. This is a standard procedure to study linearity, resolution and uniformity of a detector. It is

however insufficient to study realistic polarization measurements. We therefore used the Compton generator and beam smearing to determine the analyzing power A_0.

3.4.1 The Monte Carlo Generators

Fig. 15 shows the Compton, the beam smearing, and the combined distributions at the front face of the calorimeter, which is about 54 m away from the laser−electron interaction point. We generated 10^5 events to produce these distributions. The Compton and beam smearing generators did not only generate the locations where the gamma rays would hit the detector, but also generated the cross sections for the two helicity states, also shown in Fig. 15. Remember that the case, where the polarizations of the electron and laser beams are antiparallel, gives the large cross section at the Compton edge; this is shown with the solid line. All the distributions shown in Fig. 15 are in agreement with the analytical distributions. The one−sigma horizontal distribution due to the beam smearing is 3.77 mm and the one−sigma vertical distribution is 1.13 mm. The cross sections are also reproduced accurately within the statistical uncertainties expected for 10^5 events.

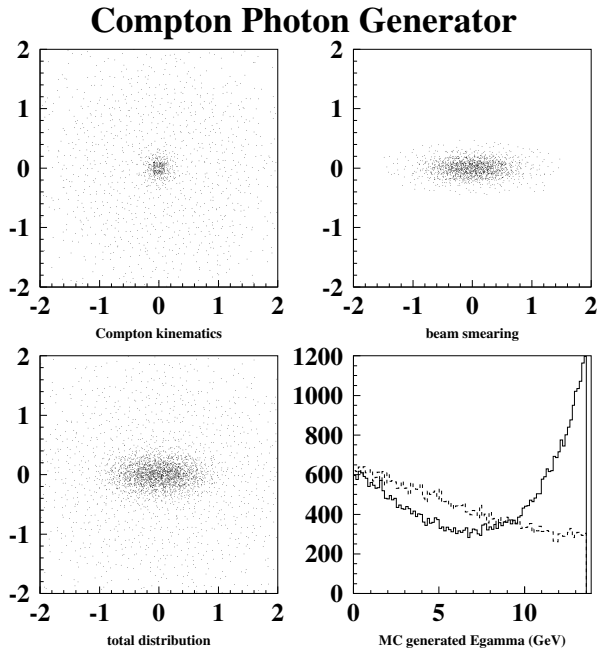

Figure 15. Top row shows 2-dim distributions (horizontal vs vertical) at the detector produced by Compton and beam smearing generators. Lower row displays the combined distribution and the gamma energy spectra for the two helicity states.

Fig. 16 shows the response of the calorimeter to the incident gamma rays. The top panel shows the case where the gamma rays are aimed at the center of the calorimeter. The bottom panel displays the extreme case, where the gamma rays are aimed at the edge of the calorimeter. In the latter case, only half of the gamma rays interact with the detector directly. Due to significant transverse leakage, the energy distribution is shifted to the left, towards lower energies. Even though the spectra are distorted and show a much lower resolution, the two helicity states are still resolved.

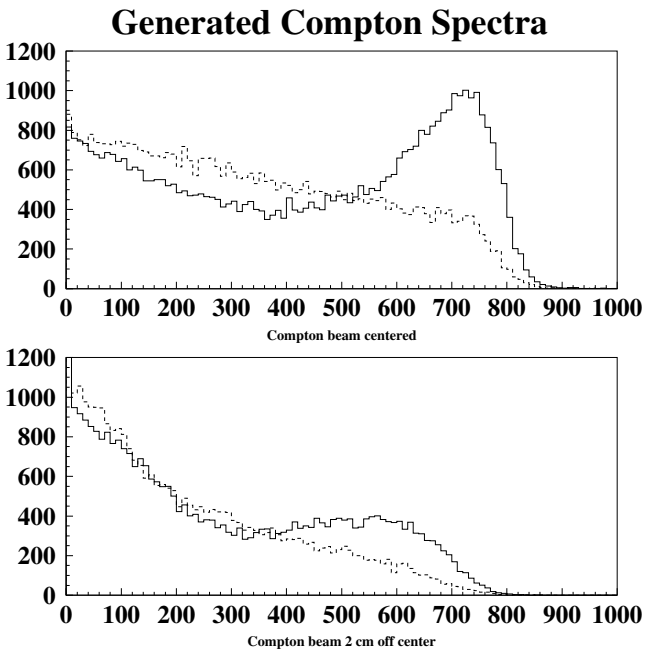

Figure 16. Top panel shows spectra for the two helicity states if Compton beam is centered on detector, whereas lower panel shows same spectra if Compton beam is aimed 2 cm off center, i.e., at the edge of the detector.

3.4.2 Checking Resolution and Uniformity

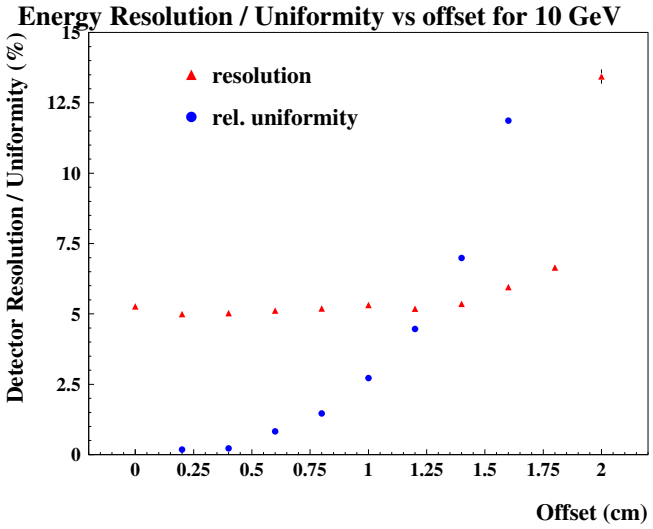

Figure 17. Resolution and relative uniformity of detector using Compton and beam smearing generators.

We also checked whether the resolution or the energy response of the detector changed if the actual Compton and beam smearing were taken into account. Since it was hard to judge from Fig. 14 how the uniformity changes as the gamma ray beam moves further away from the center, we analyzed the data in more detail. We generated a spectrum similar to the one generated in

Fig. 14, but now binned it in steps of 2 mm. We then determined the centroid and resolution for each bin. Fig. 17 shows the results of this analysis. The resolution stays flat out to about ± 14 mm. In order to determine how flat the uniformity was as a function of offset from the center, the uniformity relative to the center position is displayed in Fig. 15. Now it is straight forward to see that the detector response stays flat within 5% (10%) for ± 12.5 mm (± 15 mm).

3.4.3 Extracting the Analyzing Power A_0

We then moved on to extract the analyzing power of the detector with Compton and beam smearing included in the Monte Carlo code. To determine the longitudinal polarization of the electron beam, P_e, the asymmetry measurement is performed by switching the laser beam between left and right handed circular polarization. In the multi-Compton mode, which is studied here, this asymmetry can be written as

$$A_m(E_\gamma) = P_\lambda P_e A_0(E_\gamma), \tag{2}$$

where the analyzing power, A_0, is given by the energy weighted spectra, which here are the energy weighted cross sections folded with the detector response, for left and right handed circularly polarized light as

$$A_0 = \frac{\int \sigma(E_\gamma)_l \cdot E_\gamma \cdot \mathrm{d}E - \int \sigma(E_\gamma)_r \cdot E_\gamma \cdot \mathrm{d}E}{\int \sigma(E_\gamma)_l \cdot E_\gamma \cdot \mathrm{d}E + \int \sigma(E_\gamma)_r \cdot E_\gamma \cdot \mathrm{d}E}. \tag{3}$$

The analyzing power has a theoretical value of 0.184 for a photon energy of 2.33 eV, and an electron beam energy if 27.5 GeV. We first checked whether we could reproduce the theoretical value of 0.184 when the detector resolution was included. This was indeed confirmed to better than 0.5%, consistent with the statistical accuracy expected from the 10^5 events generated. We then went ahead and also tested how the analyzing power would change as we moved the Compton beam further and further away from the center of the calorimeter. This was done by introducing an offset in the horizontal direction. Since we ran about 10^5 events for each offset position, the generated analyzing power varied whithin statistics about 0.184, as shown in Fig. 18. Then the analyzing power was extracted from the simulated spectra. This is shown in Fig. 19. The analyzing power turned out to be astonishingly stable as a function of offset. In particular, when the analyzing power was extracted for the extreme case, where the Compton beam is aimed directly at the edge of the detector, as shown in the lower panel of Fig. 16, it turned out to be very close to the value obtained in the center, as shown in the upper panel of Fig. 16. In order to reduce the variations due to the limited statics that was produced in the Monte Carlo, the two spectra were divided. The results are shown in Fig. 20. Note, that some care must be taken when calculating error bars for the analyzing power; see details in Appendix A.

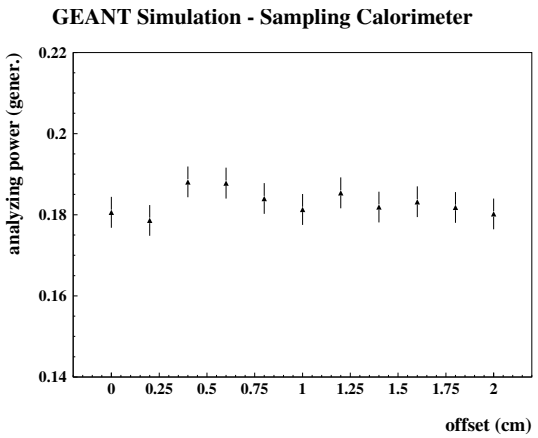

Figure 18. Analyzing power vs offset determined from initial distributions generated in Compton generator.

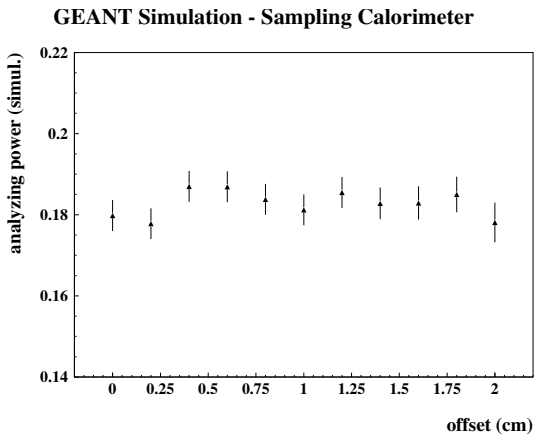

Figure 19. Analyzing power vs offset determined from simulated distributions using GEANT.

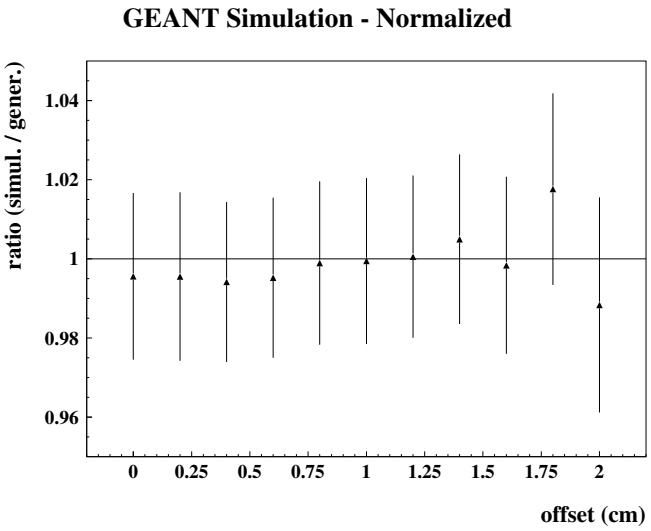

Figure 20. Ratio of GEANT simulated over Compton-generator produced distributions. This was done in an attempt to normalize the GEANT simulated distributions.

3.5 Conclusions on New Sampling Calorimeter Design

From the above simulations it is concluded that the calorimeter response is uniform within 5% in an approximately 25 mm x 25 mm area on the front face of the detector, even if realistic Compton distributions are assumed arising from Compton kinematics and electron beam divergence. Even though the detector energy response falls off rapidly as the Compton beam moves 15 mm and more away from the center position, the resolution is affected to a lesser degree, it drops off more slowly. Only if the Compton beam is moved more than 17 mm off the center does it start to drop off quickly. To our suprise, the analyzing power was even more stable than both the detector uniformity and resolution. The analyzing power was found to be stable within 0.5% for approximately ± 16 mm, and within 2%over the entire surface of the calorimeter. This makes the detector very insensitive to beam motion. For realistic running scenarios, we intend however to keep the Compton photons centered on the front face of the detector within ± 10 mm. This should be more than sufficient to get basically a position independent performance of the detector.

A Statistical Uncertainties in A_0

The error propagation of the analyzing power has to be done carefully. Taking Gaussian errors is not correct, since we have correlations in the nominator and denominator.

The analyzing power, which is a ratio of differences over sums of energy weighted spectra for left and right handed circularly polarized light, is given by

$$A_0 = \frac{L-R}{L+R} = \frac{D}{S},$$

with $L = \sum_i E_i N_i^l$ and $\delta L = \sqrt{\sum_i \left(E_i \sqrt{N_i^r}\right)^2}$, and correspondingly for R and δR.

In Gaussian error propagation, $\delta D = \sqrt{(\delta L)^2 + (\delta R)^2} = \delta S$, and the relative uncertainty in the analyzing power is then

$$\frac{\delta A_0}{A_0} = \sqrt{\left(\frac{\delta D}{D}\right)^2 + \left(\frac{\delta S}{S}\right)^2}.$$

In reality however, the terms in the nominator and denominator are not independent. Both terms, L and R appear in both, the nominator and the denominator. Since $A_0 = f(L,R)$, we have to use $\frac{d}{dL}A_0 + \frac{d}{dR}A_0$. Thus,

$$\begin{aligned} dA_0 &= \left(\frac{1}{L+R} - \frac{L-R}{(L+R)^2}\right) dL + \left(\frac{-1}{L+R} - \frac{L-R}{(L+R)^2}\right) dR \\ &= \frac{2R}{(L+R)^2} dL + \frac{-2L}{(L+R)^2} dR, \end{aligned}$$

and therefore

$$\delta A_0 = \frac{2}{(L+R)^2} \sqrt{R^2 \delta L^2 + L^2 \delta R^2}.$$

Note, however, that the two method yield the same result in the case where the analyzing power goes to zero. In fact, since the analyzing power is small, 0.184, the two methods yield almost the same result. This has been confirmed in explicit calculations. All the error bars given in Figs. 18 and 19 are calculated using the second method, which gives slightly larger error bars.